Mimosa Origami

A nanostructure-enabled directional self-organization regime of materials

Wong, William S. Y.; LI, Minfei; Nisbet, David R.; Craig, Vincent S. J.; Wang, Zuankai; Tricoli, Antonio

SOFT MATTER PHYSICS

Mimosa Origami: A nanostructure-enabled directional self-organization regime of materials

William S. Y. Wong,[1] Minfei Li,[2] David R. Nisbet,[3] Vincent S. J. Craig,[4] Zuankai Wang,[2]* Antonio Tricoli[1]*

One of the innate fundamentals of living systems is their ability to respond toward distinct stimuli by various self-organization behaviors. Despite extensive progress, the engineering of spontaneous motion in man-made inorganic materials still lacks the directionality and scale observed in nature. We report the directional self-organization of soft materials into three-dimensional geometries by the rapid propagation of a folding stimulus along a predetermined path. We engineer a unique Janus bilayer architecture with superior chemical and mechanical properties that enables the efficient transformation of surface energy into directional kinetic and elastic energies. This Janus bilayer can respond to pinpoint water stimuli by a rapid, several-centimeters-long self-assembly that is reminiscent of the *Mimosa pudica*'s leaflet folding. The Janus bilayers also shuttle water at flow rates up to two orders of magnitude higher than traditional wicking-based devices, reaching velocities of 8 cm/s and flow rates of 4.7 µl/s. This self-organization regime enables the ease of fabricating curved, bent, and split flexible channels with lengths greater than 10 cm, demonstrating immense potential for microfluidics, biosensors, and water purification applications.

INTRODUCTION

Various biological systems in nature orchestrate a high level of adaptability to their environments through the use of smart material interfaces. These can be distinguished under two overarching categories, namely, static and dynamic self-assembly (*1*, *2*). Static self-assembly is constrained by equilibrium thermodynamics (*3*). This is illustrated by the elegant self-cleaning of the lotus leaves (*4*) and the crystallization-driven (*5*) construction of intricate shells by marine invertebrates (*6*). More exciting is the dynamically responsive nature of living organisms that often manifests in spontaneous motion (*7*). For example, the *Mimosa pudica*, a thigmonastic plant, can react to the slightest contact pressure with a very rapid protective folding of its leaflets. This centimeter-long, negative tropism is transduced by a cascade of electrical potentials and osmotic pressure waves (*8*). Although the specific mechanisms vary largely, the structural and functional properties in nature exhibiting such large-scale reconfigurations provide important insights for the rational design and creation of new classes of self-organizing materials for potential applications in biotechnology (*7*), micromechanics (*9*), microelectronics (*10*), photonics (*11*), and fluidics (*1*).

To date, the engineering of inorganic systems capable of spontaneous motion relies largely on static self-organization mechanisms (*12*, *13*). In these systems, the material self-organization is localized around/in the proximity of the initial stimulus droplet, limiting the self-assembly scale. For example, in classical elastocapillarity, where a thin polymer sheet folds around a water droplet, the water droplet's surface provides both the energy for the initial folding and the propagation of the folding stimulus to the residual polymer sheet. As a result, the scale of the self-assembled structure is comparable to the

droplet size and limited to ca. 10 mm, a very small fraction of that observed in natural systems (*12*).

Here, we report the directional dynamic self-organization of soft materials into large-scale geometries by a rapid cascade folding mechanism that is reminiscent of the *M. pudica*'s leaflet folding. We engineer a hybrid Janus bilayer structure with enhanced and precisely controlled surface chemistry, morphology, and mechanical properties. These soft materials are capable of imparting directional spontaneous motion in response to a pinpoint stimulus. This self-organization mechanism relies on the rapid propagation of a pinpoint stimulus and an orthogonal local material response. The longitudinal reconfiguration (stimulus propagation) rate (maximum of 7.8 cm/s) is driven by capillary/Laplace pressure (*14*). The elastocapillary-driven orthogonal material response, observed here, has much faster kinetics (folding at ca. 23.8 cm/s) and is in line with previous studies (*15–17*). We use this system to induce the reversible self-assembly of three-dimensional (3D) microfluidic channels and spontaneous liquid self-propulsion, with velocities approaching pneumatically actuated systems. To the best of our knowledge, this Mimosa Origami regime represents the first large-scale self-assembly of a material powered by capillary-driven propagation of a pinpoint stimulus across a predetermined path.

RESULTS AND DISCUSSION

The material layout involves a stack of multifunctional layers (fig. S1, A to C) designed to impart efficient transformation of surface energy into directional kinetic and elastic energy. This is enabled through a stimulus-responsive Janus interface. The use of Janus materials has been well documented for nanoparticles, where two distinct and sometimes opposite properties, such as hydrophilic-hydrophobic, are synergistically exploited (*18*). Here, a cohesive Janus bilayer is obtained by an interconnected network of highly wettable polycaprolactone (PCL) nanofibers adhering to the bottom layer of polyvinyl chloride (PVC) microfibers (Fig. 1A). The adhesion of the PVC and PCL layers is attributed mainly to van der Waals interaction. Sequential deposition of PCL and PVP led to very weak bonding and layers that were easily

[1]Nanotechnology Research Laboratory, Research School of Engineering, The Australian National University, Canberra, Australian Capital Territory 2601, Australia. [2]Department of Mechanical and Biomedical Engineering, City University of Hong Kong, Hong Kong 999077, China. [3]Laboratory of Advanced Biomaterials, Research School of Engineering, The Australian National University, Canberra, Australian Capital Territory 2601, Australia. [4]Department of Applied Mathematics, Research School of Physics and Engineering, The Australian National University, Canberra, Australian Capital Territory 2601, Australia. *Corresponding author. Email: antonio.tricoli@anu.edu.au (A.T.); zuanwang@cityu.edu.hk (Z.W.)
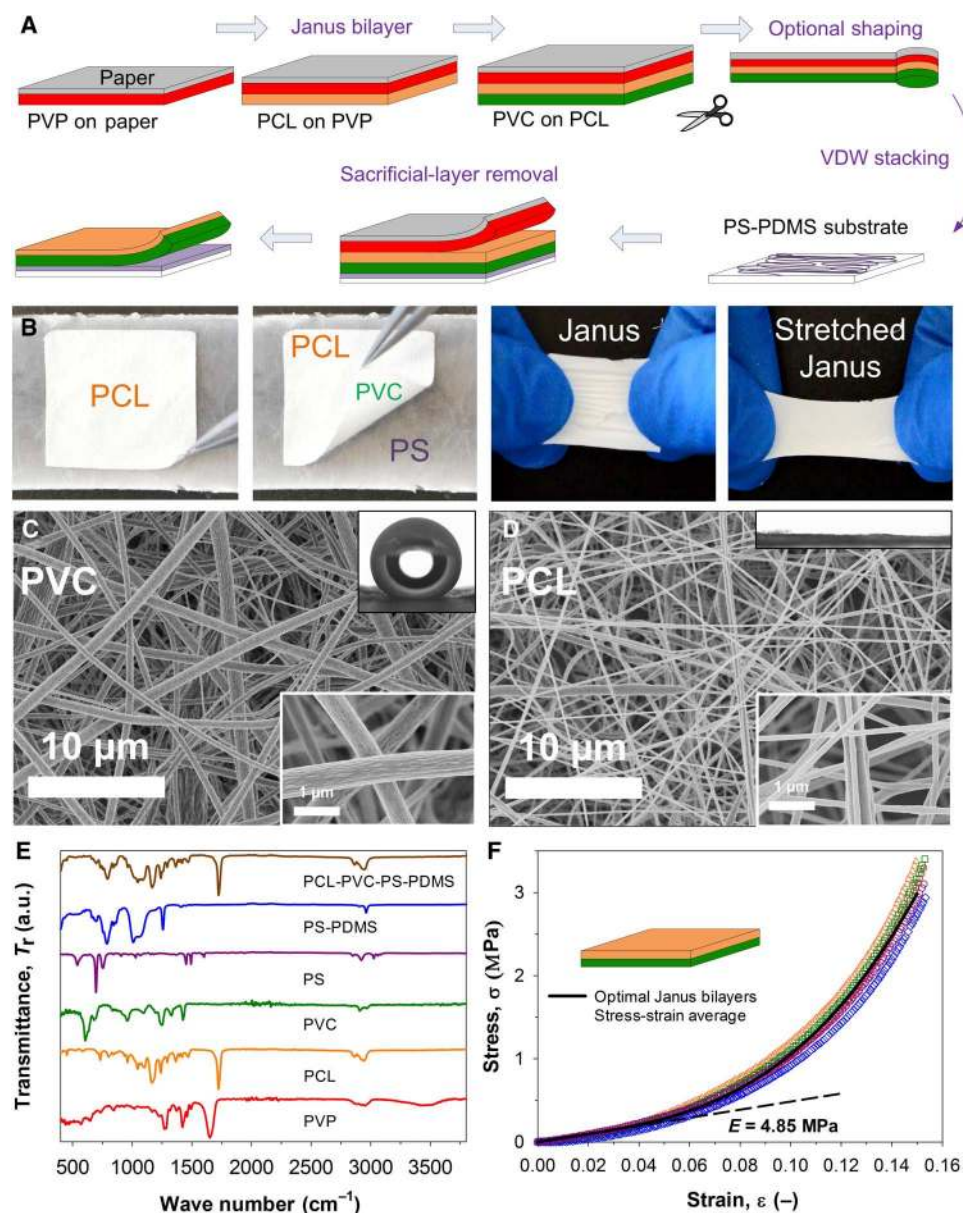
Fig. 1. Preparation and characterization of the superhydrophilic-superhydrophobic Janus bilayer. (**A**) Schematic illustration of the Janus bilayer assembly: a multifunctional stack is fabricated by sequential electrospinning of a protective PVP, a superhydrophilic PCL, and a superhydrophobic PVC nanofiber layers on paper. This stack is shaped in a functional geometry and completed by adhering a PS nanofiber layer to a flexible PDMS substrate on the PVC surface by van der Waals (VDW) interaction. The protective PVP layer and paper are easily peeled off by hand. (**B**) Optical photographs show the isolated Janus bilayer and its cohesive and stretching properties. (**C** and **D**) SEM analysis at low-magnification (8.8k) and high-magnification (70k) images (insets, bottom right) of the Janus bilayer PVC and PCL surfaces and their contrasting wetting (insets, upper right). (**E**) FTIR spectroscopic analysis of the multilayer stack and isolated Janus bilayer confirming its PCL (orange line) and PVC (green line) composition. a.u., arbitrary units. (**F**) Dynamic mechanical stress-strain analysis (tension mode) of the Janus bilayer showing a soft rubbery nature, with a Young's modulus (E) of 4.85 MPa.

peeled off, suggesting that mechanical interlocking is not the main adhesion mechanism. The PVC is designed to be highly superhydrophobic and flexible, serving as a water impenetrable backbone to the PCL layer. Moreover, to attain sufficient mobility for vertical self-organization while suppressing in-plane wrinkling, the Janus bilayer is hosted on a superhydrophobic substrate (fig. S2A) with low affinity to PVC (Fig. 1B). This substrate is composed of polystyrene (PS) nanofibers on a dense polydimethylsiloxane (PDMS) film (fig. S3A).

This multilayer stack is easily assembled on paper using a sacrificial polyvinyl pyrrolidone (PVP) layer as a protective film for the in situ deposition of the top (PCL) surface of the Janus bilayer (Fig. 1A and fig. S1). In terms of wettability, the PCL layer has a Wenzel hemiwicking (fig. S4) character, with the water contact angle approaching 0° (Fig. 1D, inset). This is achieved by the careful engineering of a network of interwoven PCL nanofibers with an average diameter of 192 ± 49 nm (Fig. 1D). Similarly, the PVC backbone of the Janus bilayer is

fabricated in situ by deposition of submicrofibers with an average diameter of 671 ± 305 nm (Fig. 1D) on the PCL layer. This porous PVC structure is superhydrophobic, with a water contact angle of 155° ± 7° and a contact angle hysteresis of 30° ± 10° (Fig. 1C, inset). The functional stack is completed by van der Waals stacking of the PS-PDMS substrate on the PVC layer. The Janus bilayer can be easily isolated from the protective PVP film (fig. S5) and the PS-PDMS substrate (Fig. 1B) by sequential peel-off. The structural integrity and composition of the isolated bilayer are confirmed by its chemical signature (Fig. 1E). The Fourier transform infrared (FTIR) spectroscopic spectra of the multilayer stack is characterized by five sharp peaks located at 1656, 1726, 612, 701, and 789 cm^{-1} that are attributed to the C=O ring of PVP, carbonyl C=O stretch of PCL, C–Cl gauche of PVC, C–H aromatic ring of PS, and Si–C with CH$_3$ rocking vibrations of PDMS, respectively ([19]). The dominant presence of PCL and the lack of PVP in the final Mimosa Origami structure (PCL-PVC-PS-PDMS) confirm successful removal of the sacrificial layers (Fig. 1E). Similarly, chemical signatures of freestanding Janus bilayers (PCL side) confirm the clean separation of Janus bilayers from the PS-PDMS substrate.

The key structural and chemical properties of the Janus bilayer, such as its elastocapillary length, surface roughness (r), and energy (E_S) can be tuned far beyond that of conventional dense polymers ([20]). Optimization of the PCL and PVC layer thickness leads to self-supported, flexible, and highly cohesive films (fig. S1B). Scanning electron microscopy (SEM) and gravimetric analysis reveal that the PCL has a surface roughness of 68 (Supplementary Materials). This is significantly higher than that ($r = 2$ to 6) achieved by microtexturing of dense films ([21]) and can be further enhanced by increasing the PCL layer thickness and decreasing the nanofiber diameter. Dynamic mechanical analysis of the optimal Janus bilayer reveals a unique rubbery stress-strain nature (Fig. 1F) with a Young's modulus of 4.85 MPa. This is two to three orders of magnitude lower than that of bulk PVC (2700 to 3000 MPa) ([22]) and PCL (252 to 430 MPa) ([23]). Considering the total PVC and PCL layers' thickness of 50 µm, this results in a very low bending rigidity (K_b) of 68 nNm and an elastocapillary length (L_{EC}) of only 1 mm, where

$$L_{EC} = \frac{K_b}{\gamma_{LV}} \quad (1)$$

and γ_{LV} is the surface energy density of water (0.072 Nm^{-1}).

Figure S6 illustrates the transient elastocapillary response of the Janus bilayer to water. When a water droplet is gently placed on the superhydrophilic side of the circular-shaped bilayer, the latter partially detaches from the PS-PDMS substrate and encapsulates it by folding symmetrically (movie S1). For a circular surface of 79 mm^2, this process takes less than 33 ms, ultimately resulting in the formation of a bulb containing the initial water volume. Note that the presence of the PS-PDMS substrate and nonwetting superhydrophobic (PVC) backbone of the Janus bilayer are also essential for the successful folding and subsequent leak-proof water encapsulation. Without the PVC layer, the non-Janus superhydrophilic PCL layer is susceptible to unwanted effects, such as uncontrolled in-plane wrinkling and eventual water leakage (figs. S7 and S8). Without the PS-PDMS substrate, the self-assembly is adversely affected by pinning to the hosting surface (figs. S7 and S8).

The rapid folding response of the Janus bilayer is attributed to its unique elastochemical properties. Notably, whereas the folding of thin dense films around a water droplet has been previously showcased as an exemplary application of elastocapillarity, here we show that utilization of highly porous layers is challenging because water leaks rapidly (fig. S7) through the hydrophilic porous structure. The superhydrophilic-hydrophobic Janus layout significantly improves the material response, avoiding wrinkling and containing the water droplet within its volume. Our rough nanostructured morphology enables significantly higher surface energy density than that of 2D textured dense films. The Janus bilayer's surface energy density was estimated at 185 J kg^{-1} (Supplementary Materials). This is comparable to that of artificial muscles ([9, 24, 25]) and large enough to easily overcome the counteracting bending rigidity (68 nNm) of the Janus bilayer. Together, this unique Janus bilayer architecture extends the working regime of classical capillary origami and renders the folding of films with more than 10 times larger thickness ([12]) while preserving a very small elastocapillary length through exceptionally high surface roughness.

The Janus bilayer's properties can be exploited to induce an unprecedented directional self-organization of soft materials into functional 3D structures. Figure 2A shows the spontaneous construction of a straight microchannel with a length of 6.5 cm. This is achieved by placing a water droplet with a diameter of 0.42 cm on the circular terminal of a rectangular strip of the Janus bilayer (figs. S5A and S9 and movie S2). This directional folding response is reminiscent of the mimosa's tropism in nature (Fig. 2B), though the stimulus propagation mechanism of the Janus bilayer is different. The reversibility of this self-organization state is achieved by reinstatement of the initial surface energy equilibrium. Figure 2C illustrates selected snapshots of the spontaneous unfolding process. Here, we used low–surface tension ethanol liquid to wet both the superhydrophobic and superhydrophilic sides of the Janus bilayer. Spectroscopy maps the surface composition of the Janus bilayers during the folding-unfolding cycles and suggests clean desorption of both water and ethanol from the material during cyclic use, with preservation of the initial chemical compositions (Fig. 2D). Subsequent desorption of the water on the PCL side restores the symmetry of the Janus bilayer surface energy (Fig. 2E) and unfolds the microchannel back into its original flat shape. The unfolded Janus bilayer is easily reactivated (Materials and Methods) and capable of multicycle self-assembly (Fig. 2, C and E).

Figure 3 (A and B) explains the mechanism of the Mimosa Origami self-assembly. A water-filled bulb initially forms (<33 ms) in response to the wetting of the Janus bilayer's circular end, and then the liquid front advances into the rectangular strip in a relatively slow manner due to the PCL layer hemiwicking character. When a critical amount of water has accumulated at the bulb-strip junction (<110 ms), the wetted strip folds into a quasi-cylindrical microchannel. The formation of this 3D hollow architecture gives rise to strong capillary force that propels water into the adjacent dry section in a rapid manner (fig. S9). Most notably, the folding signal is transported at an average rate of 400 ms cm^{-1} or an average velocity of 2.5 cm s^{-1} over a strip length of 6.5 cm. For a droplet of 40 µl and a strip width of 2 mm, the instantaneous stimulus propagation rate decreases linearly from initially 7.8 cm^{-1} to standstill over the length of 6.5 cm (Fig. 4C). Distinct from static self-organization, this axial propagation is orthogonal to the local elastocapillary potential that drives the folding of the strip. This rapid propagation of the pinpoint water stimulus and the orthogonal folding response (Fig. 3B) results in a cascade of cross-sectional folding and directional mass transport.
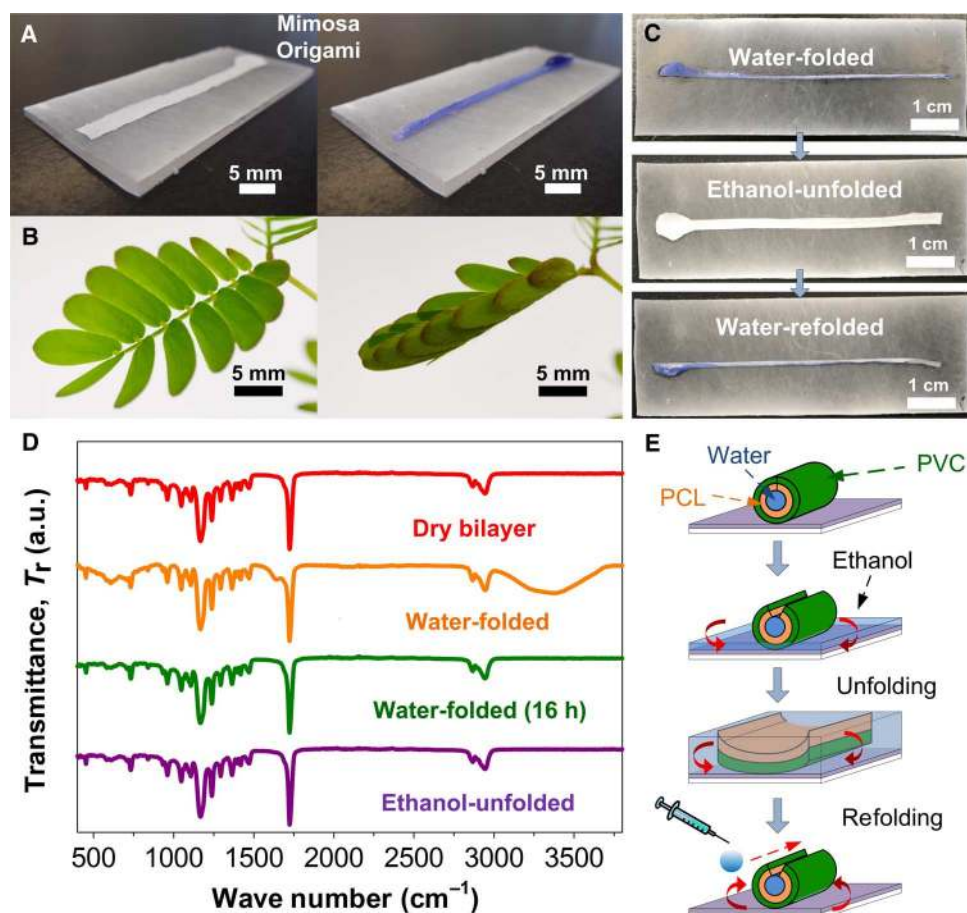
Fig. 2. Demonstration of directional self-organization via Mimosa Origami self-assembly. (**A**) Optical photographs of the spontaneous directional self-organization response of a rectangular-shaped Janus bilayer. A pinpoint water droplet stimulus results in the immediate self-assembly of a centimeter-long microchannel. (**B**) This rapid motion is reminiscent of the stimulus-response propagation during the negative tropism of the *M. pudica*'s leaflets. (**C**) The folded Janus bilayers are spontaneously unfolded by immersion in an ethanol bath. Restoration of the initial surface properties allows a novel folding cycle, demonstrating the full reversibility of this self-organization state. (**D**) FTIR spectroscopic analysis showing the variation in the surface composition of the Janus bilayer during the folding and unfolding cycle. (**E**) Schematic illustrations of capillary-induced unfolding of the self-assembled microchannel.

The effective capillary pressure decreases during self-assembly (fig. S4C). In addition, the stimulus propagation is also countered by elastic folding and viscous capillary forces. The dropping capillary pressure and increasing elastic and viscous forces decrease the stimulus propagation rate (Fig. 4C and fig. S13), ultimately halting the self-assembly, although some water is still available in the bulb. As a result, the initial scale of the self-assembly is determined by the initial droplet volume, and the self-assembly can be restarted by the supply of additional liquid to the water bulb (movies S3 and S4).

We derived a mathematical model to determine the range of material and geometrical properties for the spontaneous Mimosa Origami regime (Fig. 3C). This is based on the extension of the equations of McHale *et al.* (*15*) to an infinitesimally small length of the rectangular strip of the Janus bilayer, assuming that the top and bottom surfaces of the Janus bilayer stay in the Wenzel and Cassie-Baxter states, respectively (*15*, *16*). Material properties (Fig. 1F) and equations are described in the Supplementary Materials. We found that the spontaneous formation of a 3D hollow cross section necessitates a minimal

critical width (w_c) of the Janus bilayer strip. This critical width is a function of the elastocapillary length (L_{EC}), the characteristic contact angle (θ_e), and roughness factor (r) of the Janus bilayer top surface (*26*). It can be estimated as

$$w_c = \sqrt[2\pi]{\frac{L_{EC}^2}{1 + r\cos(\theta_e)}} \qquad (2)$$

The roughness (r) of the nanofibrous PCL layer was computed from the ratio of its total surface area to its geometric surface area, resulting in a surface roughness of 68

$$r = \frac{4m\varnothing}{\pi\rho D^2} \qquad (3)$$

where m is the mass (3.74×10^{-3} kg m^{-2}) of the monolayer PCL per m^2, $\varnothing$ is the average circumference of a nanofiber (601×10^{-9} m), ρ is the
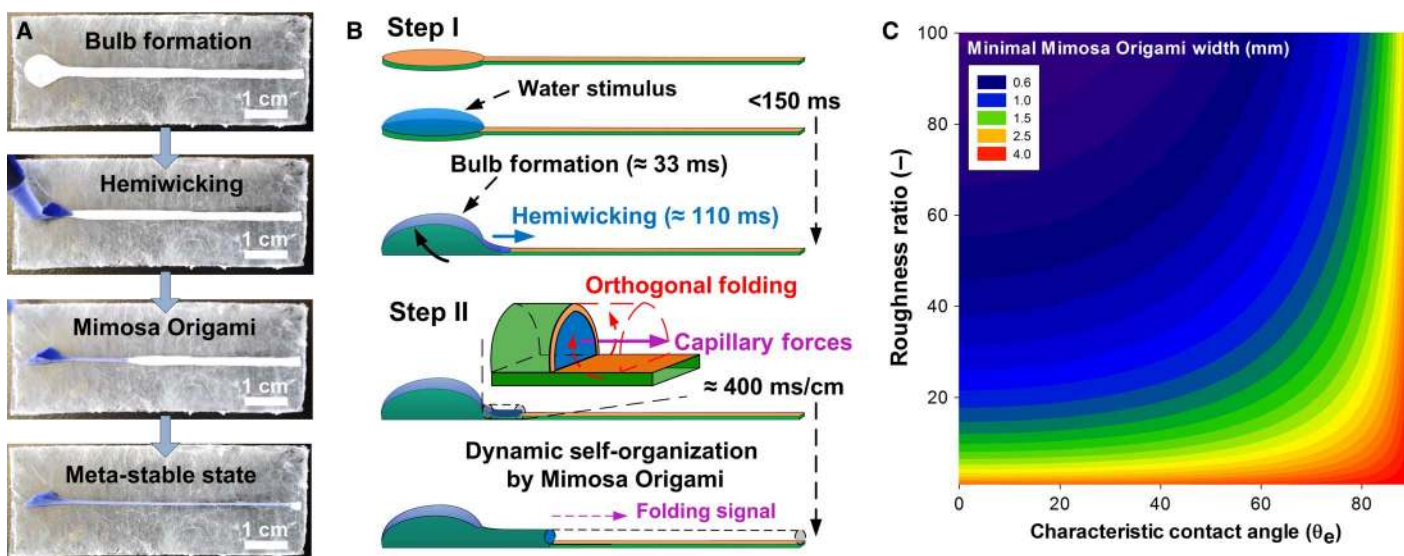
Fig. 3. Mimosa Origami self-assembly mechanism and theoretical analysis. (**A**) Optical photographs of the directional self-assembly of the Janus bilayers into a closed microchannel. (**B**) Schematic description of the self-assembly process: initially, a water-tight bulb is formed by the rapid folding (33 ms) of the Janus bilayer terminal around a water droplet. Thereafter, the waterfront slowly advances from the bulb to the dry PCL surface. Once sufficient water has collected, the wet Janus bilayer strip folds rapidly, forming a hollow 3D cross section. This leads to the Mimosa Origami propagation (400 ms cm^{-1}) of the folding stimulus by longitudinal propulsion of the waterfront and orthogonal folding of the Janus bilayer strip. (**C**) Theoretical model of the minimal strip width required for the spontaneous Mimosa Origami self-assembly regime as a function of the surface roughness and characteristic contact angle (θ_e).

density of PCL (1145 kg m^{-3}), and D is the average diameter of a nanofiber (192 × 10^{-9} m). On the basis of these calculations, the PCL layer has a surface roughness of 68.

Figure 3C shows contour plots of the minimal strip width for spontaneous folding as a function of the contact angle and roughness factor for hydrophilic films ($\theta_e < 90°$) and a constant elastocapillary length (1 mm). On the basis of this theoretical model, the minimal width for Mimosa Origami decreases significantly with increasing surface roughness (Fig. 3C). For dense flat films ($r = 1$), it is impossible to fully fold strips less than 4 mm in width. In stark contrast, for a film having comparable roughness ($r = 68$) to the top Janus bilayer surface, spontaneous complete folding is expected down to a strip width of 1.3 mm. This is extremely close to the elastocapillary length of 1 mm. As a result, for these nanorough Janus bilayers, the small amount of liquid transferred from the bulb to the dry interface by hemiwicking is sufficient to trigger the self-assembly and initiate the folding stimulus. Furthermore, it should be noted that there exists an upper limit for the strip width beyond which the self-assembled hollow cross section would partially collapse under the self-generated capillary tension.

A prompt and distal based motion that mimics the *M. pudica*'s mechanical response represents an essential improvement over state-of-the-art self-organization of soft materials (*12*). Here, we have further optimized the self-assembly kinetics by the Janus bilayer's geometrical design. For a constant water droplet volume, the maximal self-assembly length is inversely proportional to the width of the strips (Fig. 4A). This is in line with the theoretical and dynamic analysis of the self-organization process (Figs. 3 and 4B) and confirms that during Mimosa Origami, the flow is driven by the Laplace pressure of the self-assembled hollow cross section. For a rectangular strip with a width of 2 mm, the folding stimulus propagated through the complete strip length

(6.5 cm) with an average flow velocity of 2.5 cm s^{-1} (Fig. 4, A and B). Notably, for this optimal geometry, the self-assembly length is only limited by the initial size of the strip. Significantly longer lengths (ca. 200%) were easily achieved by increasing the path length (movie S4). Increasing the strip width to more than 3 mm partially disrupts the shape of the hollow cross section and decreases the maximal length of the self-assembled microchannels (Fig. 4A and movie S5). This is attributed to the partial self-collapse of the Mimosa Origami effect for strip size significantly above the elastocapillary length. The average folding-stimulus propagation velocity measured for a 2-mm-wide and 6.5-cm-long strip is 2.5 cm s^{-1}, which is comparable to the travel speeds (2 to 3 cm s^{-1}) of electrical signals in the *M. pudica* (*8*).

Remarkably, in an exemplification of bio-inspired microfluidics, the optimized Janus bilayers conveyed fluids at an estimated initial volumetric flow rate of 14.7 µl s^{-1}. This is up to 10 times faster than state-of-the-art microfluidic propulsion systems based on wicking, evaporation, and degassing (*27*). Notably, the optimal self-assembling Janus bilayer has an initial flow velocity up to 81% of that of an ideal Lucas-Washburn-Rideal (LWR) capillary due to the small delay in the time required for the self-assembly of the capillary structure. The subsequent decrease in instantaneous velocity (stimulus propagation rate) scales as the ideal LWR capillary (Fig. 4C) but eventually ceases because of the decreasing effective capillary pressure and counteracting elastic folding and viscous forces. These speeds also rival some of the fastest pumpless microfluidic devices based on etched superhydrophilic V-shaped grooves (*28*). The self-organization potential of this multilayer structure extends beyond previous studies on the utilization of water surface tension to construct complex but static 3D structures based on polymers (*12, 29*), silicon (*30*), and other materials. This is exemplified by controlling the directionality and geometry of Janus bilayer
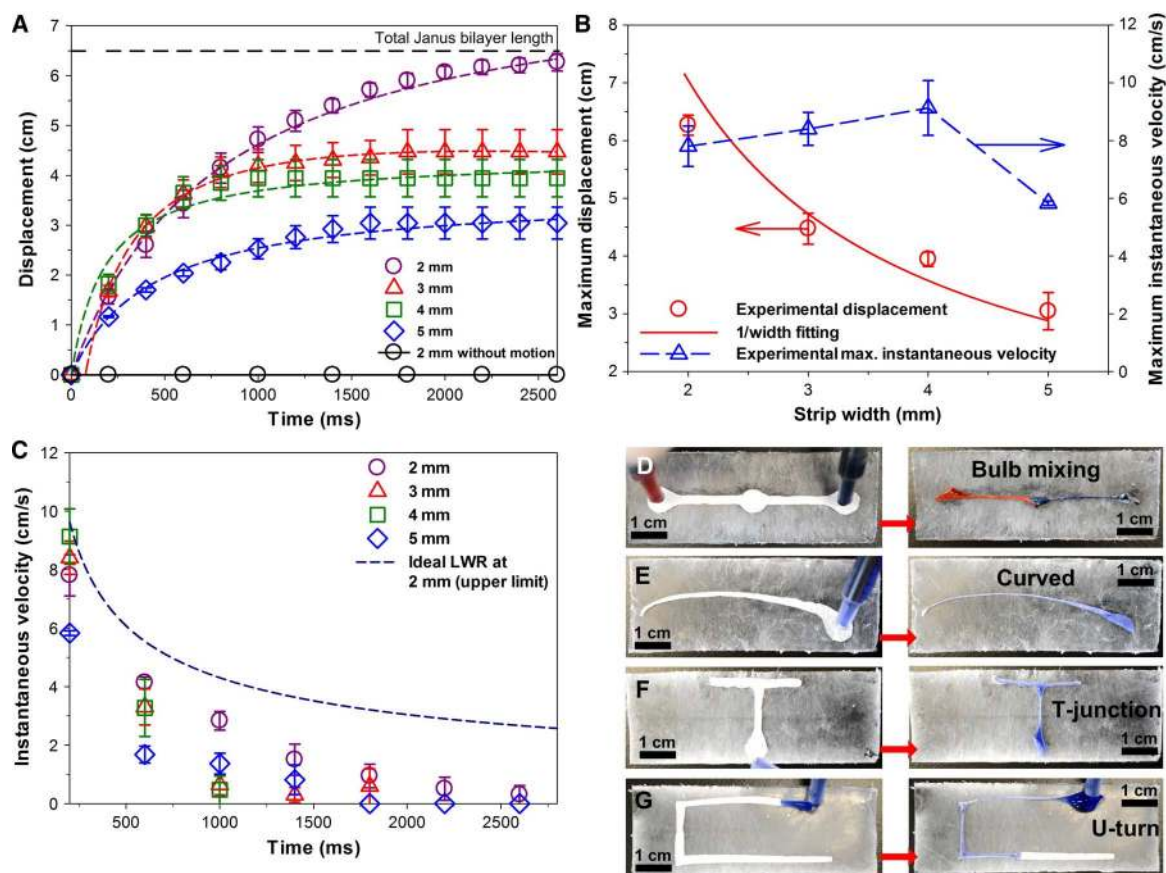
Fig. 4. Application of the Mimosa Origami directional self-organization to microfluidics. (**A**) Waterfront displacement from the bulb during Mimosa Origami self-assembly as a function of the strip width and time. (**B**) Maximal displacement and velocity as a function of strip width and 1/width fit. (**C**) Water instantaneous velocity as a function of the time since water droplet release on the Janus bilayer terminal surface and comparison against the LWR equation for an ideal circular capillary. (**D** to **G**) Exemplary modular microfluidic designs obtained by the self-assembly of functionally shaped Janus bilayer strips, including (D) mixing bulb channel, (E) curved tapering channel, (F) T junctions, and (G) U turns.

self-assembly into several functional shapes. Various key microfluidic modules with increasing degree of difficulty are easily obtained. This includes bulb mixing, tapered curves, and single and double right corners with a demonstrated self-assembly length of 10 cm (Fig. 4, D to G) that can be used for fabricating flexible modular microflow devices (Fig. 4, D to G, and movies S6 to S8). From a fundamental perspective, these structures are more than an order of magnitude larger than that previously achieved by static elastocapillary self-assembly (*12*, *31*).

CONCLUSIONS

In summary, we have demonstrated a new self-organization mechanism that, over time, enables the directional large-scale reconfiguration of soft materials. The observed self-assembly dynamics occur through a cascade of thermodynamic states that are individually accessible by dosing the water volume supplied to the Janus bilayer. As a result, this Mimosa Origami regime can overcome some of the limitations of purely elastocapillary systems and can theoretically self-assemble over unlimited lengths. Exemplification of this concept in microfluidics demonstrates record-high response time, as compared to conventional microfluidics (*27*), with near-ideal capillary velocities. Moreover, the

self-assembly is reversible, being capable of unfolding and recovering the initial surface properties. This orthogonal propagation of stimulus and response demonstrated by the Janus bilayers is a powerful mechanism that can be exploited in numerous research areas and commercial applications, including stimuli-responsive materials (*10*, *32*), fog harvesting (*33*), artificial muscles (*9*, *25*), sensors (*34*), switches (*32*), and power-independent devices (*18*).

MATERIALS AND METHODS

Polymer solution preparation
PVP solutions were made by dissolving 0.789 g of PVP (Sigma-Aldrich, M_w = 1,300,000) in 10 ml of ethanol (Sigma-Aldrich, anhydrous, ≥99.5%). PCL solutions were made by dissolving 0.948 g of PCL (Sigma-Aldrich, M_n = 80,000) in 9 ml of chloroform (Sigma-Aldrich, anhydrous, ≥99%) and 3 ml of methanol (Sigma-Aldrich, anhydrous, ≥99.8%). PVC solutions were made by dissolving 1.335 g of PVC (Sigma-Aldrich, M_w = 80,000) in 10 ml of tetrahydrofuran (Sigma-Aldrich, anhydrous, ≥99.9%). PS solutions were made by dissolving 0.944 g of PS (Sigma-Aldrich, M_w = 280,000) in 10 ml of N,N-dimethyl formamide (Sigma-Aldrich, anhydrous, ≥99.8%). Dodecyltrimethylammonium

bromide (DTAB; Sigma-Aldrich, ≥98%) was added to the PVP, PCL, PVC, and PS solutions at concentrations of 1.1, 3.0, 1.1, and 1.9 mg ml^{-1}, respectively.

Substrate preparation

PDMS substrates were prepared using Sylgard 184 (Dow Corning), which is composed of a 10:1 ratio of base elastomer to curing agent. These were mixed together, degassed, and cast as rectangular PDMS slides with a dimension of $75 \times 25 \times 1$ mm. Full curing of the substrates was conducted at 70°C overnight (16 hours) in a convection oven (MTI). Laboratory paper towel (Kimberly-Clark, Scott Towel Roll) and cardboard (OfficeMax) substrates were used without further treatment.

Electrospinning of the Janus bilayers, protective PVP layer, and dewetting PS-PDMS substrate

A horizontal electrospinning setup was used, with a spinning drum diameter of 10 cm and a rotation of 300 to 400 rpm. The optimal electrospinning of all layers (PVC, PCL, and PVP) on paper towel (sacrificial substrate) was achieved by systematic optimization of key synthesis parameter matrix over an electrode working distance of 10 to 15 cm, an electric potential of 5 to 30 kV, a solution concentration of 2 to 30 w/w, a DTAB concentration of 0 to 2 mg ml^{-1}, and a polymer solution feed rate of 0.5 to 2.0 ml hour^{-1}. The optimization was aimed at producing pure beadless nanofibrous layers with desired wetting (PCL) and dewetting (PVC) properties. As a result of this optimization, PVP nanofibers were electrospun at a working distance and flow rate of 10.5 cm and 1.2 ml hour^{-1}, with an applied voltage of 25 kV for 1 hour. PCL nanofibers were electrospun at a working distance and flow rate of 15 cm and 1.5 ml hour^{-1}, with an applied voltage of 15 kV for 1 hour as the primary functional layer. PVC nanofibers were electrospun at a working distance and flow rate of 10 cm and 1.0 ml hour^{-1}, with an applied voltage of 25 kV for 2 hours as the encapsulation layer. The addition of DTAB aided the synthesis of pure nanofibrous layers through the enhancement of charge densities in the jet stream (35). DTAB-aided electrospinning of PVP and PVC did not experience extreme wetting variations, whereas PCL films electrospun under the influence of DTAB were observed to develop a highly hydrophilic interface, outlined by hemiwicking properties. In contrast, PCL nanofibrous layers electrospun without DTAB exhibited hydrophobic properties that were in close alignment with the current literature (36). The well-integrated PVC-PCL nanofibrous layers constituted the Janus bilayer. The trilayer (with PVP) was developed between 50 and 60% relative humidity. As-developed trilayers were then encased in aluminum foil and kept in a dry desiccated environment, enabling the preservation of its Janus functionality over extended periods (tested up to 6 months).

Electrospinning of the PS nanofibrous layer on PDMS was likewise optimized over a range of electrospinning parameters (see above), and was subsequently conducted using a vertical electrospinning setup (Electrospunra ES-210), at a working distance and flow rate of 10 cm and 1.0 ml hour^{-1}, with an applied voltage of 25 kV for 6 min between 30 and 50% relative humidity. A lateral travel distance of 7 cm with a speed of 2 cm s^{-1} was used to improve homogeneity. The PS nanofibers developed on PDMS were not moisture-sensitive and could be stored indefinitely without loss in functionality.

Shaping of the Janus bilayers

The as-developed multilayered nanofibrous films were shaped into the desired mimosa bilayer strips by cutting them across printed templates designed with a graphics software. Template shapes included straight and curved channels and single and double right-angled turns, as well as a variety of mixing channels. The minimum Janus bilayer strip width tested here was 2 mm. The low adhesion between the PVP protective layer and the Janus bilayer enabled clean and easy removal of the paper substrate and PVP layer, resulting in a freestanding functional strip (fig. S5A). Alternatively, the surface properties of the Janus bilayer were enhanced by exposing peeled bilayers (PCL side) to water plasma for 3 min at 50 W, resulting in superhydrophilic-superhydrophobic Janus bilayers. These Janus bilayer strips were thereafter placed onto several substrates, including polymers, papers, and nanofibrous materials.

Mechanical and surface analysis of the Janus bilayer

The mechanical properties of the Janus bilayer were determined through a series of stress-strain tests using a dynamical mechanical analyzer (DMA 8000, PerkinElmer) with a tension-rectangle mode and a maximum load of 5 N at 0.2 N min^{-1}, a frequency of 1 Hz, and a force multiplier of 1 at a controlled temperature of 25°C. The Young's modulus was computed from five repeats of the linear region of the corrected stress-strain curve, with a strain of 0 to 0.04 mm (Fig. 1F).

The thicknesses of the Janus bilayers placed on PDMS were measured via a white-light interferometer (Veeco, Wyko NT9100). The vertical scanning interferometry mode was used at ×50 magnification with a field of view of 1×. A backscan of 50 µm with a scan length of 100 µm was used, with a modulation of 2%.

The film roughness (r) was computed as the ratio between the actual surface area and geometrical surface area by gravimetric analysis (PerkinElmer, STA 8000), and SEM assisted fiber diameter counts over ca. 9 cm^2 in the geometrical surface area for three cross-batch samples.

Morphological and chemical analysis

All the nanofiber layers were analyzed with a Zeiss UltraPlus analytical scanning electron microscope (field-emission SEM) at 3 kV. Before SEM, the specimens were platinum sputter–coated for 2 min at 20 mA. Fiber diameters were computed using ImageJ with 50 counts for each sample. Data were presented as means ± SDs. FTIR attenuated total reflectance was performed with a Bruker Alpha FTIR (Bruker) at 24 scans from 400 to 4000 cm^{-1} on all samples.

Wetting analysis

The wetting properties of the Janus bilayer were assessed by contact angle (CA) measurements using a CA goniometer with a rotary stage. Dynamic and static images were recorded using a KSV CAM200 CA goniometer with a heliopan ES43 camera. The PS-PDMS superhydrophobic substrates were tested as-prepared, whereas the Janus bilayers were initially laminated onto sticky PDMS substrates before testing. Static CAs were measured using the sessile drop (5 µl) technique averaged over five repeats. Sliding angles (SAs) were determined by placing a 10-µl drop of deionized water directly on sample surfaces before tilting via a goniometer. Results were averaged across three readings. Contact angle hysteresis (CAH) was measured via the drop-in drop-out technique, which provided the average advancing contact angle between 8 and 9 µl and the average receding contact angle between 1 and 2 µl. An average was determined over five repeats. Dynamic CAs were measured for the PCL side of the Janus bilayer. The CAs, SAs, and CAHs were computed by a commercially available (CAM2008) program. Data are presented as means ± SDs.

Wong *et al. Sci. Adv.* 2016;2:e1600417   24 June 2016

7 of 9

Analysis of the Mimosa Origami self-assembly

The directional self-organization of the Janus bilayers was assessed on the PS-PDMS substrate. Deionized water was dyed red and blue using Congo red (Sigma-Aldrich, 35% dye content), methylene blue (Sigma-Aldrich, ≥82% dye content), and trypan blue (Sigma-Aldrich, 60% dye content) at concentrations of 1.5, 1.5, and 0.25 mg ml^{-1}, respectively, to aid visualization. Mimosa Origami strips were approximately 6.5 cm in length. Strip widths of between 2 and 5 mm were used in conjunction with an actuation bulb of 7 mm in diameter. Mimosa Origami was initiated through a single 40-μl droplet deposited on the actuation bulb. A digital single-lens reflex camera (Nikon D3200) was used to capture the dynamic origami at a resolution of 720p and 60 fps. Movies captured were then imported into Microsoft Movie Maker and analyzed at sequential frames of 30 ms. Repeatability was assessed through five different cross-batch repeats. Tests were conducted at approximately 20° to 25°C and between 50 and 70% relative humidity. Spontaneous unfolding of Mimosa Origami–assembled microchannels was observed by immersing the as-folded channels into a dish of ethanol. Surface wetting of the PVC side enabled a symmetrical restoration of the Janus bilayers' surface energies, enabling spontaneous disassembly. The unfolded channels were then lifted out of the ethanol and dried in a desiccated environment overnight before plasma reactivation (20 W, 1 min). Modular microfluidic-type channels (tapered curves, right-angled turns, and mixing channels) were also tested via the simultaneous deposition of colored microdroplets. Results demonstrated potential for the simple development of templated, single-step self-assembled microfluidic devices (movies S6 to S9). Pump-aided inflation-deflation cycles were executed with a 10-ml syringe (Terumo) on a syringe pump (New Era Pump Systems) operating at 10 ml hour^{-1} to showcase suitability of pumped microfluidics.

SUPPLEMENTARY MATERIALS

Supplementary material for this article is available at http://advances.sciencemag.org/cgi/content/full/2/6/e1600417/DC1

Supplementary Text
Supplementary Calculations
Supplementary Material Data
Supplementary Equations
fig. S1. Synthesis of nanostructured Janus bilayer by sequential electrospinning.
fig. S2. SA analysis of the superhydrophobic layers.
fig. S3. Morphological characterization (SEM) of the supporting and sacrificial layers.
fig. S4. Hemiwicking superhydrophilic nature of the PCL layer.
fig. S5. Separation of the Janus bilayer from the PVP protective layer.
fig. S6. Static self-assembly of Janus bilayers.
fig. S7. Janus bilayer and PCL monolayer response on hydrophilic (paper) substrates.
fig. S8. Qualitative wetting characterization of 2- and 3-mm strips of Janus bilayer and PCL monolayer on a hydrophilic paperboard.
fig. S9. Enlarged images of initial Janus bilayer folding.
fig. S10. Representative thermodynamic states of the Janus bilayer during self-assembly.
fig. S11. Response of the PVC side of the Janus bilayer to water.
fig. S12. Mimosa Origami of a 2-mm strip of Janus bilayer and PCL monolayer on the PDMS-PS substrates.
fig. S13. Decreasing stimulus propagation rate for a 2-mm-wide strip and a stimulus droplet size of 40 μl.
table. S1. Width-to-diameter ratios of Mimosa Origami–assembled microchannels.
table. S2. Material properties of Janus bilayers.
movie S1. Static self-assembling properties of circular-shaped Janus bilayer demonstrating artificial tropism in response to a microdroplet.
movie S2. Mimosa Origami assembly of the Janus bilayer strips on a superhydrophobic PS-PDMS substrate.
movie S3. Mimosa Origami assembly of the Janus bilayer strips performing double right-angle turns on a superhydrophobic PS-PDMS substrate.

movie S4. Mimosa Origami assembly of the Janus bilayer strips performing longer and tighter double right-angle turns on a superhydrophobic PS-PDMS substrate.
movie S5. Mimosa Origami assembly of the Janus bilayer strips on a superhydrophobic PS-PDMS substrate.
movie S6. Modular microfluidics: Janus-based Mimosa Origami strips with double-ended bulbs on a superhydrophobic PS-PDMS substrate showing in-channel droplet mixing.
movie S7. Modular microfluidics: Janus-based Mimosa Origami strips with double-ended bulbs, with a central bulb on a superhydrophobic PS-PDMS substrate, showing in-bulb droplet mixing.
movie S8. Modular microfluidics: Janus-based Mimosa Origami strips at a T-junction, showcasing double-ended split for potential in multichannel capabilities.
movie S9. Cyclic insertion and removal of water from an as-assembled microfluidics channel, showcasing suitability toward pump-aided microfluidic designs.
References (37–44)

REFERENCES AND NOTES

1. J. V. I. Timonen, M. Latikka, L. Leibler, R. H. A. Ras, O. Ikkala, Switchable static and dynamic self-assembly of magnetic droplets on superhydrophobic surfaces. *Science* **341**, 253–257 (2013).
2. G. M. Whitesides, B. Grzybowski, Self-assembly at all scales. *Science* **295**, 2418–2421 (2002).
3. J. S. Moore, M. L. Kraft, Synchronized self-assembly. *Science* **320**, 620–621 (2008).
4. A. Tuteja, W. Choi, M. Ma, J. M. Mabry, S. A. Mazzella, G. C. Rutledge, G. H. McKinley, R. E. Cohen, Designing superoleophobic surfaces. *Science* **318**, 1618–1622 (2007).
5. W. L. Noorduin, A. Grinthal, L. Mahadevan, J. Aizenberg, Rationally designed complex, hierarchical microarchitectures. *Science* **340**, 832–837 (2013).
6. M. Suzuki, M. Suzuki, K. Saruwatari, T. Kogure, Y. Yumamoto, T. Nishimura, T. Kato, H. Nagasawa, An acidic matrix protein, Pif, is a key macromolecule for nacre formation. *Science* **325**, 1388–1390 (2009).
7. J. R. Capadona, K. Shanmuganathan, D. J. Tyler, S. J. Rowan, C. Weder, Stimuli-responsive polymer nanocomposites inspired by the sea cucumber dermis. *Science* **319**, 1370–1374 (2008).
8. A. G. Volkov, J. C. Foster, V. S. Markin, Signal transduction in *Mimosa pudica*: Biologically closed electrical circuits. *Plant Cell Environ.* **33**, 816–827 (2010).
9. M. Ma, L. Guo, D. G. Anderson, R. Langer, Bio-inspired polymer composite actuator and generator driven by water gradients. *Science* **339**, 186–189 (2013).
10. S. Xu, Z. Yan, K.-I. Jang, W. Huang, H. Fu, J. Kim, Z. Wei, M. Flavin, J. McCracken, R. Wang, A. Badea, Y. Liu, D. Xiao, G. Zhou, J. Lee, H. U. Chung, H. Cheng, W. Ren, A. Banks, X. Li, U. Paik, R. G. Nuzzo, Y. Huang, Y. Zhang, J. A. Rogers, Assembly of micro/nanomaterials into complex, three-dimensional architectures by compressive buckling. *Science* **347**, 154–159 (2015).
11. Y. A. Vlasov, X.-Z. Bo, J. C. Sturm, D. J. Norris, On-chip natural assembly of silicon photonic bandgap crystals. *Nature* **414**, 289–293 (2001).
12. J. D. Paulsen, V. Démery, C. D. Santagelo, T. P. Russell, B. Davidovitch, N. Menon, Optimal wrapping of liquid droplets with ultrathin sheets. *Nat. Mater.* **14**, 1206–1209 (2015).
13. J. Boekhoven, W. E. Hendriksen, G. J. M. Koper, R. Eelkema, J. H. van Esch, Transient assembly of active materials fueled by a chemical reaction. *Science* **349**, 1075–1079 (2015).
14. E. W. Washburn, The dynamics of capillary flow. *Phys. Rev.* **17**, 273 (1921).
15. G. McHale, M. I. Newton, N. J. Shirtcliffe, N. R. Geraldi, Capillary origami: Superhydrophobic ribbon surfaces and liquid marbles. *Beilstein J. Nanotechnol.* **2**, 145–151 (2011).
16. G. McHale, All solids, including teflon, are hydrophilic (to some extent), but some have roughness induced hydrophobic tendencies. *Langmuir* **25**, 7185–7187 (2009).
17. C. Py, P. Reverdy, L. Doppler, J. Bico, B. Roman, C. N. Baroud, Capillary origami: Spontaneous wrapping of a droplet with an elastic sheet. *Phys. Rev. Lett.* **98**, 156103 (2007).
18. X. Pang, C. Wan, M. Wang, Z. Lin, Strictly biphasic soft and hard Janus structures: Synthesis, properties, and applications. *Angew. Chem. Int. Ed.* **53**, 5524–5538 (2014).
19. N. B. Colthup, L. H. Daly, S. E. Wiberley, *Introduction to Infrared and Raman Spectroscopy* (Academic Press, London, ed. 3, 1990).
20. D. Quéré, Wetting and roughness. *Annu. Rev. Mater. Res.* **38**, 71–99 (2008).
21. B. Bhushan, Y. Chae Jung, Wetting study of patterned surfaces for superhydrophobicity. *Ultramicroscopy* **107**, 1033–1041 (2007).
22. P. T. Anastas, W. Leitner, P. G. Jessop, *Handbook of Green Chemistry, Green Solvents, Supercritical Solvents* (Wiley, Weinheim, Germany, 2014), vol. 4.
23. S. Eshraghi, S. Das, Mechanical and microstructural properties of polycaprolactone scaffolds with one-dimensional, two-dimensional, and three-dimensional orthogonally oriented porous architectures produced by selective laser sintering. *Acta Biomater.* **6**, 2467–2476 (2010).
24. Q. M. Zhang, V. Bharti, X. Zhao, Giant electrostriction and relaxor ferroelectric behavior in electron-irradiated poly(vinylidene fluoride-trifluoroethylene) copolymer. *Science* **280**, 2101–2104 (1998).
25. M. Shahinpoor, Micro-electro-mechanics of ionic polymeric gels as electrically controllable artificial muscles. *J. Intell. Mat. Syst. Str.* **6**, 307–314 (1995).

26. R. N. Wenzel, Resistance of solid surfaces to wetting by water. *Ind. Eng. Chem.* **28**, 988–994 (1936).

27. X. Wang, J. A. Hagen, I. Papautsky, Paper pump for passive and programmable transport. *Biomicrofluidics* **7**, 14107 (2013).

28. J. Tian, D. Kannangara, X. Li, W. Shen, Capillary driven low-cost V-groove microfluidic device with high sample transport efficiency. *Lab Chip* **10**, 2258–2264 (2010).

29. C. Py, P. Reverdy, L. Doppler, J. Rico, B. Roman, C. N. Baroud, Capillarity induced folding of elastic sheets. *Eur. Phys. J. Spec. Top.* **166**, 67–71 (2009).

30. X. Guo, H. Li, B. Y. Ahn, E. B. Duoss, K. J. Hsia, J. A. Lewis, R. G. Nuzzo, Two- and three-dimensional folding of thin film single-crystalline silicon for photovoltaic power applications. *Proc. Natl. Acad. Sci. U.S.A.* **106**, 20149–20154 (2009).

31. L. Gao, T. J. McCarthy, Teflon is hydrophilic. Comments on definitions of hydrophobic, shear versus tensile hydrophobicity, and wettability characterization. *Langmuir* **24**, 9183–9188 (2008).

32. S.-W. Hwang, S.-K. Kang, M. A. Brenckle, F. G. Omenetto, J. A. Rogers, Materials for programmed, functional transformation in transient electronic systems. *Adv. Mater.* **27**, 47–52 (2015).

33. R. P. Garrod, L. G. Harris, W. C. E. Schofield, J. McGettrick, L. J. Ward, D. O. H. Teare, J. P. S. Badyal, Mimicking a Stenocara beetle's back for microcondensation using plasma-chemical patterned superhydrophobic-superhydrophilic surfaces. *Langmuir* **23**, 689–693 (2006).

34. A. W. Martinez, S. T. Phillips, G. M. Whitesides, E. Carrilho, Diagnostics for the developing world: Microfluidic paper-based analytical devices. *Anal. Chem.* **82**, 3–10 (2009).

35. P. T. Hammond, in *Colloids and Colloid Assemblies: Synthesis, Modification, Organization and Utilization of Colloid Particles*, F. Caruso, Ed. (Wiley, Weinheim, Germany, 2003), pp. 317–341.

36. F. Chen, C. N. Lee, S. H. Teoh, Nanofibrous modification on ultra-thin poly(e-caprolactone) membrane via electrospinning. *Mater. Sci. Eng. C* **27**, 325–332 (2007).

37. W. S. Y. Wong, N. Nasiri, A. L. Rodriguez, D. R. Nisbet, A. Tricoli, Hierarchical amorphous nanofibers for transparent inherently super-hydrophilic coatings. *J. Mater. Chem. A* **2**, 15575–15581 (2014).

38. C. Ishino, K. Okumura, Wetting transitions on textured hydrophilic surfaces. *Eur. Phys. J. E Soft Matter* **25**, 415–424 (2008).

39. C. Ishino, M. Reyssat, E. Reyssat, K. Okumura, D. Quéré, Wicking within forests of micropillars. *Europhys. Lett.* **79**, 56005 (2007).

40. M.-H. Zhao, X.-P. Chen, Q. Wang, Wetting failure of hydrophilic surfaces promoted by surface roughness. *Sci. Rep.* **4**, 5376 (2014).

41. L. Liu, S. Guo, J. CHang, C. Ning, C. Dong, D. Yan, Surface modification of polycaprolactone membrane via layer-by-layer deposition for promoting blood compatibility. *J. Biomed. Mater. Res. Part B Appl. Biomater.* **87**, 244–250 (2008).

42. C. Wan, B. Chen, Reinforcement and interphase of polymer/graphene oxide nanocomposites. *J. Mater. Chem.* **22**, 3637–3646 (2012).

43. T. D. Brown, A. Slotosch, L. Thibaudeau, A. Tauberger, D. Loessner, C. Vaquette, P. D. Dalton, D. W. Hutmacher, Design and fabrication of tubular scaffolds via direct writing in a melt electrospinning mode. *Biointerphases* **7**, 13 (2012).

44. L. A. Girifalco, R. J. Good, A theory for the estimation of surface and interfacial energies. I. Derivation and application to interfacial tension. *J. Phys. Chem.* **61**, 904–909 (1957).

Science Advances

Mimosa Origami: A nanostructure-enabled directional self-organization regime of materials

William S. Y. Wong, Minfei Li, David R. Nisbet, Vincent S. J. Craig, Zuankai Wang and Antonio Tricoli

ARTICLE TOOLS	http://advances.sciencemag.org/content/2/6/e1600417
SUPPLEMENTARY MATERIALS	http://advances.sciencemag.org/content/suppl/2016/06/21/2.6.e1600417.DC1
REFERENCES	This article cites 41 articles, 12 of which you can access for free http://advances.sciencemag.org/content/2/6/e1600417#BIBL
PERMISSIONS	http://www.sciencemag.org/help/reprints-and-permissions

Use of this article is subject to the Terms of Service